Hindawi
Journal of Chemistry
Volume 2022, Article ID 3137142, 11 pages
https://doi.org/10.1155/2022/3137142

Research Article

Synthesis and Antitumor Activity of a GSH Inert Bisphosphonate Platinum (II) Complex

Lu Ma,[1,2,3] **Hua Liu**,[4] **Yichun Ju**,[5] **Kai Chen**,[6] **Yi Yang**,[7] **Zhichao Zhou**,[7] **Zhenqin Zhang**,[5] **and Zheng Cai**[5]

[1]*Department of Periodontology, The Affiliated Stomatological Hospital of Nanjing Medical University, Nanjing 210029, China*
[2]*Jiangsu Province Key Laboratory of Oral Diseases, Nanjing 210029, China*
[3]*Jiangsu Province Engineering Research Center of Stomatological Translational Medicine, Nanjing 210029, China*
[4]*School of Chemistry and Chemical Engineering, Anshun University, Anshun 561000, China*
[5]*School of Pharmacy, Nanjing Medical University, Nanjing 211166, China*
[6]*Collaborative Innovation Center of Atmospheric Environment and Equipment Technology, Jiangsu Key Laboratory of Atmospheric Environment Monitoring and Pollution Control, Nanjing University of Information Science & Technology, Nanjing 210044, China*
[7]*Changzhou Vocational Institute of Engineering, Changzhou 213164, China*

Correspondence should be addressed to Zhenqin Zhang; zhangzhq@njmu.edu.cn and Zheng Cai; caizheng@njmu.edu.cn

Received 10 June 2022; Revised 5 September 2022; Accepted 23 September 2022; Published 7 October 2022

Academic Editor: Maria F. Carvalho

Copyright © 2022 Lu Ma et al. This is an open access article distributed under the Creative Commons Attribution License, which permits unrestricted use, distribution, and reproduction in any medium, provided the original work is properly cited.

Osteosarcoma is a highly aggressive neoplasm. Traditional platinum chemotherapeutic agents for osteosarcoma inevitably have acquired drug resistance and serious side effects, which have limited their utility. To slow down the reaction of platinum drugs with glutathione (GSH) is a strategy to overcome the resistance of platinum chemotherapeutic agents. Herein, the unique design of a GSH inert bisphosphonate platinum complex cis-{di(amino)platinum[tetraethyl 2,2-bis(2-pyridinylmethyl)methylidene-1,1-bisphosphonate]} (DBPP) is reported. MTT assay demonstrates that DBPP showed moderate inhibition towards human osteosarcoma cell line U2OS cells. The cytostatic action of DBPP is related to conformational conversion from B-DNA to A-DNA and the unwinding of pUC19 DNA. DBPP could also destroy the tertiary structure of human serum albumin (HSA). Notably, ^{31}P NMR and ^{1}H NMR indicate that DBPP can hardly chelate with GSH, which could overcome the GSH-induced side effects. We envision that this unique design of the platinum complex would open up new ways to overcome GSH-induced resistance.

1. Introduction

Osteosarcoma is a highly aggressive neoplasm that majorly occurs in patients younger than 25 years or older than 59 years [1, 2]. Annual incidence is estimated at 2–4 patients per million [1, 3]. Osteosarcoma arises from mesenchymal cells producing osteoid and/or bone, especially located in the long bones of the extremities [4–6]. The osteosarcoma cells show biological heterogeneity because of karyotypes that accompany patients for several months, and up to 30% of newly diagnosed patients will develop metastases [7, 8]. For those patients with metastatic or recurrent disease, therapeutic outcomes remain unsatisfactory, and the overall 5 years survival rate remains poorly at 20% [9, 10]. Therefore, it is urgent to develop more effective treatments for osteosarcoma.

Current clinical treatment of osteosarcoma is mainly based on neoadjuvant chemotherapy followed by surgery plus postoperative radiotherapy and chemotherapy [4]. The past decades have witnessed the effective improvement of osteosarcoma prognosis by using platinum chemotherapeutic agents such as cisplatin, which has improved 5-year survival rates for osteosarcoma to 60%–80% [11, 12]. The main mechanism of cisplatin is the inhibition of proliferation of rapidly dividing cells through DNA damage [13, 14]. After aquation inside cells, the platinum atom of cisplatin

binds covalently to the N7 position of purines and DNA interstrand cross-linking occurs, which interferes with DNA synthesis, replication, and transcription, which is mainly responsible for the anticancer efficacy of platinum drugs [15]. However, the acquired drug resistance and severe side effects of cisplatin are inevitable and limit its utility [16].

A number of strategies, including structural modification in the platinum (II) coordination sphere, have been used to combat the resistance associated with platinum drugs [17]. For instance, the steric bulk ligand present around the platinum center enables the anticancer drug picoplatin to bypass platinum resistance by inhibiting cisplatin-resistant cell lines including human ovarian carcinoma xenograft ADJ/PC6cisR, L1210cisR, and CH1cisR [18]. The second example is N, N-chelate Pt (II) complexes, which possess micromolar activity in H460 cells. Another benefit of N, N-chelate Pt (II) complexes is that they prevent platinum from reacting with GSH [19, 20]. Therefore, well-designed platinum (II) complexes not only significantly advance our understanding of platinum complexes but also increase the likelihood that we will be able to overcome cellular resistance associated with platinum-based complexes.

The most widely known bone-targeting agents used in the formation of Pt complexes are bisphosphonates (BPs), which have been used to treat bone diseases such as osteoporosis, bone metastases, and multiple myeloma [21–24]. In view of these fascinating effects, Pt-BPs complexes with appealing characteristics have been explored. Particularly, the Pt-BPs complexes were discovered to have lower acute toxicity than the conventional drug cisplatin and preferentially inhibit osteosarcoma in *in vitro* studies [25, 26]. Some of the Pt-BPs complexes have been exploited as dual-targeting agents [26, 27].

Herein, we report the design, synthesis, and characterization of a bisphosphonate platinum complex, DBPP. In order to inherit the merits of reported Pt-BPs, we continue to use bisphosphonate as the nonleaving ligand. Considering that bis-or tridentate amine ligands could slow down the nucleophilic reactions by GSH [19], we adopted the strategy of employing bi-nitrogen pyridine ligands in DBPP. We evaluated and discussed the biological properties of DBPP through the investigation of their lipophilicity, accumulation, cytotoxicity, DNA, and HSA binding. We further demonstrate the stability of DBPP in the presence of GSH. This study provides a new strategy to overcome GSH-induced resistance.

2. Experimental

2.1. Materials, Measurements, and Data Analysis. Cisplatin, (3-(4, 5-dimethylthiazol-2-yl)-2,5-diphenyl tetrazolium bromide (MTT), 2-(chloromethyl)pyridine hydrochloride, human serum albumin (HSA), and L-glutathione (GSH) were purchased from sigma. Supercoiled pUC19 plasmid DNA and 6X loading buffer (0.05% bromophenol blue, 0.035% xylene cyanol FF, 36% glycerol, and 20 mM EDTA) were purchased from Takara Biotechnology (Dalian) Co., Ltd. Calf thymus DNA (CT-DNA), Tris and ethidium bromide (EB) were purchased from Sunshine Bio. Co., Ltd (Nanjing, China). All chemicals were used as received without further purification unless otherwise stated. The human osteosarcoma cell lines U2OS and MG-63, the human breast carcinoma cell line MCF-7 and the human cervical cancer cell line HeLa were originated from the Cancer Institute & Hospital, Chinese Academy of Medical Sciences.

Anhydrous N, N-dimethylformamide (DMF), and dimethylsulfoxide (DMSO) were prepared by refluxing or stirring the commercial reagent in the presence of calcium hydride for 72 hours. 2-[2-pyridinylethylidene]bis[phosphonic acid] tetraethyl ester was synthesized according to the previous literature [26].

The ^{1}H, ^{13}C, ^{31}P, and ^{195}Pt NMR spectra were acquired on a Bruker DRX-500 spectrometer. Electrospray ionization mass spectrometry (ESI-MS) spectra were recorded using the LCQ fleet ESI-MS spectrometer (Thermo Scientific), and the isotopic distribution pattern for the complex was simulated using the ISOPRO 3.0 program. Elemental analyses were carried out with Elementar Vario ELIII. FT-IR spectra were recorded on a Tensor-27 FT-IR spectrometer (Bruker, Germany) with a resolution of 2 cm^{-1} and a spectral range of 4000–400 cm^{-1}. The high-performance liquid chromatography (HPLC) sample was centrifuged, and the supernatant was subjected to analysis at 220 nm *via* an SPD-20AV Shimadzu HPLC instrument equipped with a C18 reverse-phase column (eluent: 50/50 H_2O/CH_3OH). The circular dichroism (CD) experiments were performed on a Jasco J-810 spectropolarimeter (Japan Spectroscopic, Japan) in a 1 cm path length cylindrical quartz cell at room temperature. The UV-vis spectra were determined on a Shimadzu UV 3600 (UV-vis-near-IR) spectrophotometer. The images of agarose gel electrophoresis were obtained by using a Bio-Rad Gel-Doc XR imaging system, and quantification analysis was performed with *Quantity One software*. The inductively coupled plasma mass spectrometry (ICP-MS) data were obtained on ELAN9000 ICP-MS (PerkinElmer Inc., U. S. A.). The optical density (OD) of formazan was tested on ThermoScientific Varioskan Flash.

All cell experiments were conducted in triplicate. Statistical analyses were performed with the SPSS software. Data were expressed as the mean ± standard deviation.

2.2. Synthesis of Tetraethyl 2,2-Bis(2-Pyridinylmethyl) Methylidene-1,1-Bisphosphonate (Ligand). 2-Chloromethyl pyridine hydrochloride (5.292 g, 32 mmol) was dissolved in water (7 mL), and the solution was made alkaline by adding sodium hydroxide (1.344 g, 32 mmol) to water (14 mL). The mixture was extracted with chloroform, the extract was dried over anhydrous $MgSO_4$ and the solvent was removed in vacuo. The residue was purified by vacuum distillation to give 2-chloromethyl pyridine as a pale red oil. In a separate bottle, 2-[2-pyridinylethylidene]bis(phosphonic acid) tetraethyl ester (9.31 g, 24.56 mmol) in 20 mL dry DMSO was added to a mixture of 60% N (1.08 g, 29.47 mmol) in DMSO 20 mL at 0°C under nitrogen. The reaction mixture was stirred at 0°C for 30 min then at room temperature for 2 h. 2-

Chloromethylpyridine (2.82 g, 20 mmol) was then added dropwise to the stirring reaction mixture. The reaction was allowed to stir for an additional 96 h at room temperature and then quenched by the addition of saturated aqueous ammonium chloride. The reaction mixture was extracted with methylene chloride, and the organic extracts were combined and concentrated under reduced pressure. The mixture was redissolved in excess toluene, washed with H_2O and brine, dried over Na_2SO_4, and concentrated under a vacuum. The yellow product is purified by flash chromatography with isopropyl alcohol in methylene chloride in silica gel. ^{1}H NMR (500 MHz, $CDCl_3$): δ 8.60 (*s*, 2 H), 7.77 (*d*, $J = 7.74$ Hz, 2 H), 7.58 (*t*, $J = 7.42$ Hz, 2 H), 7.15 (*s*, 2 H), 4.02–3.97 (*m*, 8 H), 3.64 (dd, $J = 12.15$, 2.58 Hz, 4 H), and 1.12 (td, $J = 7.05$, 2.03 Hz, 12 H). ^{13}C NMR (125 MHz, $CDCl_3$): δ 158.14, 148.37, 135.39, 126.55, 121.43, 62.46, 50.55, 36.71, and 16.16. ^{31}P NMR (202 MHz, $CDCl_3$): δ 23.84. IR (KBr) cm^{-1}: 3431, 2977, 2930, 2869, 1624, 1584, 1470, 1437, 1390, 1356, 1250, 1022, 968, 874, 807, 686, 613, and 513. ESI-MS (*m/z*, positive mode). Found (calcd): $[Ma + H]^+$, 471.33 (471.44), $[2M + Na]^+$, and 963.17 (963.88).

2.3. Synthesis of DBPP. Cisplatin (75 mg, 0.25 mmol) and $AgNO_3$ (42.5 mg, 0.25 mmol) were stirred in anhydrous DMF (4.0 mL) in the dark at 40°C for 24 h. The resulting AgCl precipitate was removed by filtration and Ligand (94.27 mg, 0.2 mmol) was added to the filtrate. After stirring for an additional 24 h at 40°C, $AgNO_3$ (34.0 mg, 0.20 mmol) was added to the solution, and the solution was stirred for another 24 h at 40°C. The resulting AgCl precipitate was removed by filtration, and CH_2Cl_2 (100 mL) was added to the reaction mixture. The white precipitate was removed by filtration and the filtrate was evaporated under reduced pressure. The resulting oil was dissolved in $CHCl_3$ (4 mL) and added to diethyl ether (100 mL). A yellow precipitate of DBPP was formed at a 58% yield. ^{1}H NMR (500 MHz, $CDCl_3$): δ 9.44 (*s*, 2 H), 7.68 (*t*, $J = 7.85$ Hz, 2 H), 7.58 (*d*, $J = 7.75$ Hz, 2 H), 7.45 (*t*, $J = 5.04$ Hz, 2 H), 5.05 (*s*, 4 H),4.42 (*m*, 6 H), 4.11 (*t*, $J = 13.56$ Hz, 2 H), 3.67 (*s*, 4 H), 1.87 (*s*, 6 H), and 1.50 (*t*, $J = 7.01$ Hz, 6 H); ^{13}C NMR (125 MHz, $CDCl_3$): δ 161.02, 152.68, 138.44, 129.96, 125.19, 64.77, 42.26, 16.55, and 15.70; ^{31}P NMR (202 MHz, $CDCl_3$): δ 22.88, 20.55; ^{195}Pt NMR (107 MHz, $CDCl_3$): δ−2287.651. IR (KBr) cm^{-1}: 3433, 3225, 2990, 1611, 1484, 1443, 1376, 1356, 1223, 1049, 968, 780, 653, 607, and 533. ESI-MS (*m/z*, positive mode). $[C_{21}H_{38}N_4O_6P_2Pt]^+$ found (calcd.): 698.33 (699.19); $[C_{21}H_{38}N_4O_6P_2Pt]^{2+}$ found (calcd.): 349.92 (349.59). Calculated for $C_{21}H_{38}N_6O_{12}P_2Pt$: C, 30.62; H, 4.65; N, 10.20. Found: C, 30.68; H, 4.42; N, 10.13%. The purity of DBPP was determined to be >98% by HPLC. The retention time was 5.07 minute.

2.4. Computational Modeling. Electronic properties of the chemical structures of the ligand and DBPP were calculated using density functional theory (DFT). In particular, the hybrid functional B3LYP, electron basis sets 6-311G (*d*, *p*), and an effective core potential LanL2DZ basis set as implemented in the Gaussian09 suite of programs were used for full geometry optimization. In all calculations, the integral equation form (IEFPCM) of the polarization continuum model was used to simulate the solvent (water) environment. The frequencies of all geometries are calculated at the same level. HOMO (highest occupied molecular orbital) and LUMO (lowest unoccupied molecular orbital) were calculated for the optimized geometries.

2.5. Anticancer Activity Assays. The *in vitro* MTT assay was carried out according to a previously reported procedure [28]. Briefly, the U2OS (osteosarcoma), MG-63 (osteosarcoma), MCF-7 (breast carcinoma), and HeLa (cervical cancer) cells were inoculated in 96-well plates and incubated in different media. U2OS was maintained in DMEM with 10% fetal bovine serum. MG-63, MCF-7, and HeLa cells were maintained in RPMI 1640 medium with 10% fetal bovine serum. These cells were cultured at 37°C in an atmosphere of 5% CO_2 and 95% air and 100% relative humidity overnight. After plating, different concentrations of DBPP in PBS were added to the above culture medium. After the cells were incubated for another 48 h, MTT (20 μL, 5 mg mL^{-1} in PBS) was added to each well. After another 4 h of incubation, the culture plates were centrifuged, and the medium was removed. Then DMSO (200 μL) was added to each well, and the absorbance of dissolved formazan was measured at 570 nm by an ELISA plate reader. The inhibition rate (%) or IC_{50} was the mean of three independent results.

2.6. Lipophilicity Determination. Lipophilicity determination was carried out by using the 1-octanol/buffer system of the shake-flask method [29]. Briefly, solutions of DBPP (50, 100, 150, and 200 μM) were prepared in the phosphate buffer (10 mM, pH 7.4) which was presaturated with 1-octanol. 2.0 mL of the solution and equal volumes of 1-octanol were mixed and placed in a thermostatic (25.0 ± 0.1°C) air-bath orbital shaker at 200 rpm for 4 h. After centrifugation at 2500 rpm for 15 min, the samples were separated into two phases. According to the law of mass conservation, the concentration of the solute in the aqueous phase was determined by spectrophotometry ($\lambda_{max} = 267$ nm). The drug concentration of the corresponding 1-octanol phase and the lipo-hydro partition coefficient $P_{o/w}$ ($C_{o/Cw} = A_o/A_w$), where A stands for absorbance) were calculated.

2.7. Platinum Cellular Uptake. U2OS cells (15×10^4) were seeded in 6-well plates, which were allowed to grow for 18 h, then treated with DBPP (50.0 μM and 100.0 μM) for 24 h, 48 h, and 72 h, respectively. After incubation, the medium was removed and all of the wells were washed with phosphate-buffered saline (PBS) three times. The cells were trypsinized, and live cells were counted by the trypan blue method. After that, cells were suspended in 500 μL PBS and digested with 0.5 mL of hot (≈95°C) concentrated nitric acid for 2 h, followed by the addition of H_2O_2 (50 μL) and HCl (100 μL). The obtained homogenized solution was diluted by water and analyzed by ICP-MS to determine the total platinum content per well. The amount of platinum was

calculated by subtracting the average amount of platinum found in the blank wells from the average amount of platinum found in the cell-containing wells and normalizing it to the average number of cells per well.

2.8. Studies on DNA Interaction. The DNA binding experiments were performed in Tris-HCl/NaCl buffer (5 mM Tris-HCl, 50 mM NaCl, pH 7.4) using different concentrations of DBPP. After CT-DNA was incubated with different ratios of DBPP at 37°C for 24 h in the dark, CD spectra were recorded in the wavelength range of 220–320 nm. Each CD spectrum was recorded after averaging over at least 3 accumulations, and the buffer background was subtracted.

The impact on the secondary structure of plasmid DNA was determined by agarose gel electrophoresis. pUC19 plasmid DNA (200 ng) was treated with different concentrations of DPP at 37°C for 24 h. All the samples were finally loaded onto a 1% agarose gel containing EB ($0.5\,\mu g{\cdot}mL^{-1}$). Electrophoresis was carried out for 2 h at 100 V in a TAE buffer (50 mM Tris-acetate and 1 mM ethylenediaminetetraacetic acid). The resulting bands were visualized under UV light. The resulting photographs were obtained by using a Bio-Rad Gel-Doc XR imaging system.

2.9. Interaction with HSA. Reactions of DBPP with HSA were carried out in PBS (10 mM, pH 7.4). Reactions were monitored by UV-Vis and absorption spectra were obtained after HSA (3.0 μM) with different concentrations of DBPP in PBS at 37°C for 24 h in the dark.

2.10. Solubility Test. Solubility testing was carried out using distilled water and chloroform as test media. Each test was repeated 3 times. One milliliter of each test medium was put in a glass tube and stirred with a constant speed of 80 rpm for 10 min after the start of the test. Then, the samples were incubated at 37°C for 30 min and centrifuged for 10 min at 10,000 rpm. The solvent of each sample was removed, and the dry sample was redissolved in 1.0 mL of distilled water. The platinum concentration of the samples was determined by ICP-MS. The dissolution values were calculated and expressed in the form of Mol/L (M).

2.11. Stability of DBPP. DBPP (*ca.* 0.0056 mmol) was dissolved in a solution of deuterated aqueous and placed into an NMR tube. GSH (2.45 mg, *ca.* 0.0132 mmol) was added to the same NMR tube. Then, the tube was kept at 37°C, and the obtained solution was monitored by ^{1}H NMR and ^{31}P NMR at different time intervals.

3. Results and Discussion

3.1. Characterization. Preparation of DBPP was conducted according to the procedure shown in Scheme 1. Briefly, the ligand was straightforwardly obtained from nucleophilic substitution reaction of 2-(chloromethyl)pyridine hydrochloride and 2-[2-pyridinylethylidene]bis(phosphonic acid) tetraethyl ester. Then, the ligand was reacted with cationic *cis*-$[Pt(NH_3)_2Cl(DMF)]^+$, after which $AgNO_3$ was added to afford DBPP in high yield. Since there are two pyridyl rings in DBPP, it is assumed that DBPP is more difficult to react with GSH. In addition, the coordination of the ligand with platinum (II) affords an eight-membered ring. To the best of our knowledge, it is the first example reported till now.

The ligand and the resulting platinum complex (DBPP) have been characterized by using NMR, ESI-MS, and IR spectroscopy. Compared to the free ligand, the aromatic proton signals in the ^{1}H NMR data of DBPP significantly shift to a lower field, indicating that the pyridine nitrogen has been coordinated to the Pt^{II} center. Additionally, ^{31}P NMR data of the free ligand provided a singlet at 23.84 ppm, whereas two new signals at 22.88 and 20.55 ppm were observed for the DBPP indicating a change in the P atoms' signals as a result of coordination with platinum. Moreover, the ^{195}Pt NMR signal from DBPP falling at −2287.651 ppm further confirmed that the Pt^{II} complex was successfully developed. The IR spectrum of the ligand and DBPP complex showed a POO-stretching band in the 1000–1250 region [30]. The ESI-MS spectrum of DBPP showed two main peaks at m/z 349.92 and 698.33, which could be ascribed to the positively charged species $[C_{21}H_{38}N_4O_6P_2Pt]^{2+}$ and $[C_{21}H_{38}N_4O_6P_2Pt]^{+}$, respectively.

3.2. DFT Calculation. We carried out the DFT calculation using a collection of Gaussian 09 programs in order to theoretically comprehend the coordination of DBPP [31–33]. Figure 1 demonstrates how the central Pt^{2+} coordinates with two N atoms from NH_3 and two N atoms from the pyridine units, the latter of which almost stand in a straight line in opposite directions. Figure 1 also displays the spatial distributions of the HOMO and LUMO of the ligand and DBPP. The ligand's electron density, whether HOMO or LUMO, is evenly distributed, primarily on the pyridine unit. In contrast, the majority of the electrons in the HOMO orbital are distributed on the N-Pt binding site in the DBPP upon binding with platinum ions. Additionally, DBPP's energy gap (E) between HOMO and LUMO is 3.28 eV, lower than the ligand's (5.98 eV), indicating that DBPP is more stable than the free ligand.

3.3. Antiproliferative Activity. The cytotoxic potency of DBPP was evaluated. As shown in Table 1, DBPP did not show significant activity against MG-63, MCF-7, and HeLa cell lines at a concentration of 50 and 100 μM after 24 h incubation. However, DBPP exhibits a significant inhibitory effect on U2OS cells' ability to proliferate, indicating a higher selectivity than cisplatin. The high systemic toxicity of cisplatin is thought to be associated with nonselectivity [34]. By redirecting drugs at the specific site of injury or disease is the most promising strategy to compel the associated drug

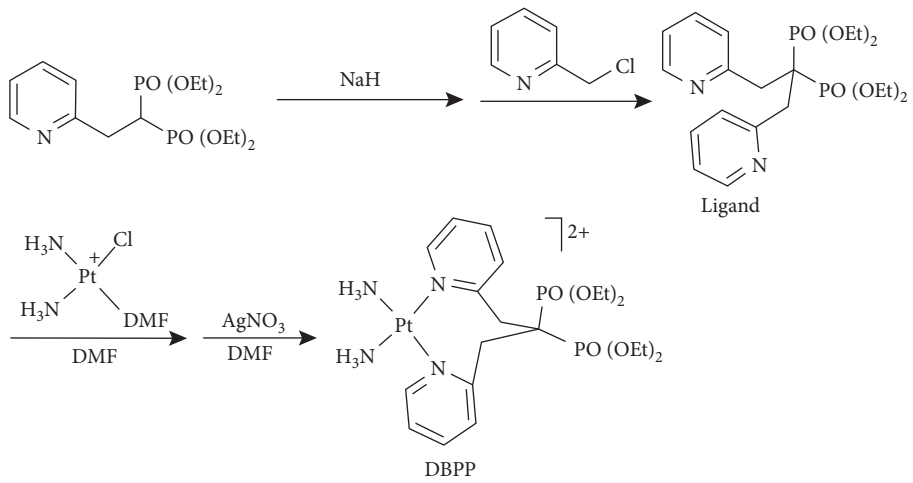

Scheme 1: Synthesis of DBPP.

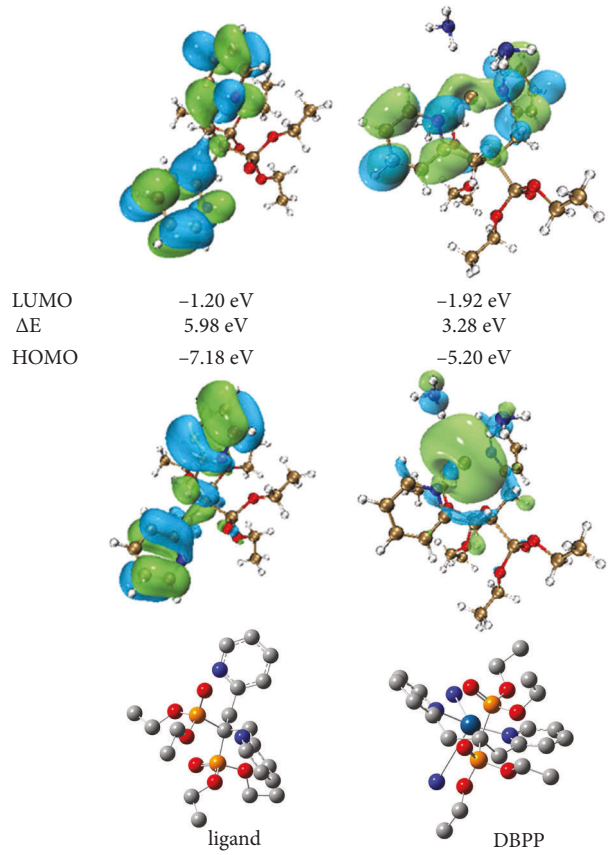

Figure 1: The molecular structure, HOMO, and LUMO of the ligand and DBPP by DFT calculation.

Table 1: Relative cellular viability of DBPP for 24 h[a].

Cell	Relative cellular viability at 50.0 μM concentration	Relative cellular viability at 100.0 μM concentration
MG-63	100.0% ± 2.5%	85.9% ± 1.8%
U2OS	85.8% ± 1.6%	55.7% ± 3.0%
HeLa	100.0% ± 1.1%	100.0% ± 1.6%
MCF-7	100.0% ± 0.9%	100.0% ± 3.8%

[a]Relative cellular viability of cisplatin toward MG-63, U2OS, HeLa, and MCF-7 at 10.0 μM concentration for 24 h is 59.0% ± 1.0%, 52.1% ± 2.2%, 48.5% ± 1.0%, and 51.2% ± 1.2%, respectively.

resistance and may be helpful in lowering systematic toxicities [35]. The difference in selectivity between DBPP and cisplatin may be due to the presence of a bisphosphonate moiety in DBPP as opposed to cisplatin.

At the concentration of 50 and 100 μM, the relative cellular viability is 85.8% ± 1.6% and 55.7% ± 3.0%, respectively (Table 1). With the extension of incubation time from 24 h to 48 h, the relative cellular viability reduced to 65.6% ± 3.8% and 48.2% ± 0.9%, respectively. When the incubation time was extended to 72 h, the relative cellular viability reduced to 58.3% ± 4.8% and 30.7% ± 1.6%, respectively (Table 2). The 50% inhibition appeared at concentrations up to about 60 μM. In contrast, cisplatin was more cytotoxic. For example, the relative cellular viability of cisplatin toward MG-63 at 10.0 μM concentration for 24 h is 59.0% ± 1.0%.

Analysis of the structure-activity relationship revealed that the leaving group has an important influence on the cytotoxicity. The result of cytotoxicity indicated that DBPP which has no leaving group in the structure, shows moderate cytotoxicity against U2OS cells but is quite less potent than cisplatin and BPP, the latter of which have at least one leaving the group in the structure [26].

3.4. Lipophilicity and Cellular Uptake. The lipophilicity parameter (log P) is a crucial factor in membrane transport [36, 37]. Here, the log P value of DBPP was determined as water-octanol partition coefficients using the shake-flask method. The log P is calculated to be -1.1 ± 0.1 (Figure 2), showing that DBPP is more lipophilic than BPP (log $P = -1.7$) [26] and cisplatin (log $P = -2.3$) [38].

The U2OS cellular uptake of DBPP was determined by ICP-MS. When U2OS cells were treated with 10.0 μM cisplatin for 24 h, the concentration of cellular was 2.6 ± 0.2 μg/10^6 cells. However, treating U2OS cells with 50.0 μM of DBPP for 24 h only resulted in 0.6 ± 0.5 μg/10^6 cells concentration of cellular platinum (Table 3), which was quite lower than that of cisplatin. Prolonging the incubation time to 48 h or 72 h could not bring about a significant increase in cell uptake. After exposure to 100.0 μM of DBPP for 48 and 72 h, the concentration of cellular platinum rose to 3.7 ± 0.5 and 5.0 ± 0.3 μg/10^6 cells, respectively. In addition, the results indicate that the Pt uptake is correlated with the cytotoxicity.

3.5. Interaction with DNA. Since DNA is the primary target of Pt (II)-based antitumor complexes, to get more insight into the antitumor activity of DBPP, the ability of DBPP to bind calf thymus DNA (CT-DNA) and unwind supercoiled pUC19 DNA was investigated. Figure 3(a) displays the circular dichroism CD spectra of CT-DNA in the absence or presence of varying amounts of DBPP, where the negative band at 245 nm and the positive one at 275 nm represent the characteristics of B-DNA. With the rising of the [DBPP]/[DNA] ratio from 0 to 0.8, the intensity of the negative bands decreases and the positive bands increases. Moreover, the maximum wavelength of the negative bands has a tendency to redshift. Such a changing tendency indicates a conformational conversion from B-DNA to A-DNA. The changes of the negative and positive bands are quite similar to that of DNA modified by cisplatin and this suggests that DBPP can induce a similar formation of intrastrand cross-links with cis-$[PtCl_2(Py)_2]$ [39]. Figure 3(b) shows the DNA unwinding property of DBPP by native agarose gel electrophoresis using pUC19 DNA. Upon incubation with DBPP, retardation of supercoiled DNA was observed, indicating untwisting by DNA binding. Additionally, the separation between supercoiled and relaxed DNA decreases as the molar ratio (r_i) increases. The coalescence point r_i (c) for complete removal of supercoiled DNA is 1.8, which is higher than that of cisplatin (r_i (c) = 0.076) [40]. The results suggest that DBPP cannot perturb the tertiary structure of supercoiled DNA as efficiently as cisplatin, which is consistent with their cytotoxicity.

Table 2: Relative cellular viability of DBPP toward U2OS at 24, 48, and 72 h.

Concentration (μM)	Relative cellular viability		
	24 h	48 h	72 h
50.0	85.8% ± 1.6%	65.6% ± 3.8%	58.3% ± 4.8%
100.0	55.7% ± 3.0%	48.2% ± 0.9%	30.7% ± 1.6%

3.6. Interaction with HSA. HSA plays a crucial role in the transport of drugs because of its remarkable binding properties and the highest abundance in blood plasma [41]. UV-Vis spectrophotometry was used as a simple method to explore the interaction of DBPP with HSA. The effect of DBPP on the UV-Vis absorption of HSA is shown in Figure 4. With the addition of DBPP, the absorption intensity of HSA was enhanced with an obvious blue shift of about 12 nm (from 278 to 266 nm) indicating that the microenvironment of tryptophan (Trp), tyrosine (Tyr), and phenylalanine (Phe) residues were altered and they were extended into the aqueous milieu [42]. These observations confirm that DBPP can destroy the tertiary structure of HSA and form a novel complex with HSA.

3.7. Stability of DBPP. Having the U2OS selectively inhibited platinum complex in hand, we next turned our attention to investigating the reactivity between DBPP and Glutathione (GSH). GSH is a soluble tripeptide whose intracellular concentrations are between 0.5 to 10 mM. As a nucleophilic molecule, GSH could chelate with platinum (II) to form a Pt $(GS)_2$ conjugate, which is then exported out of the cells. It would decrease the platinum (II)-mediated DNA damage

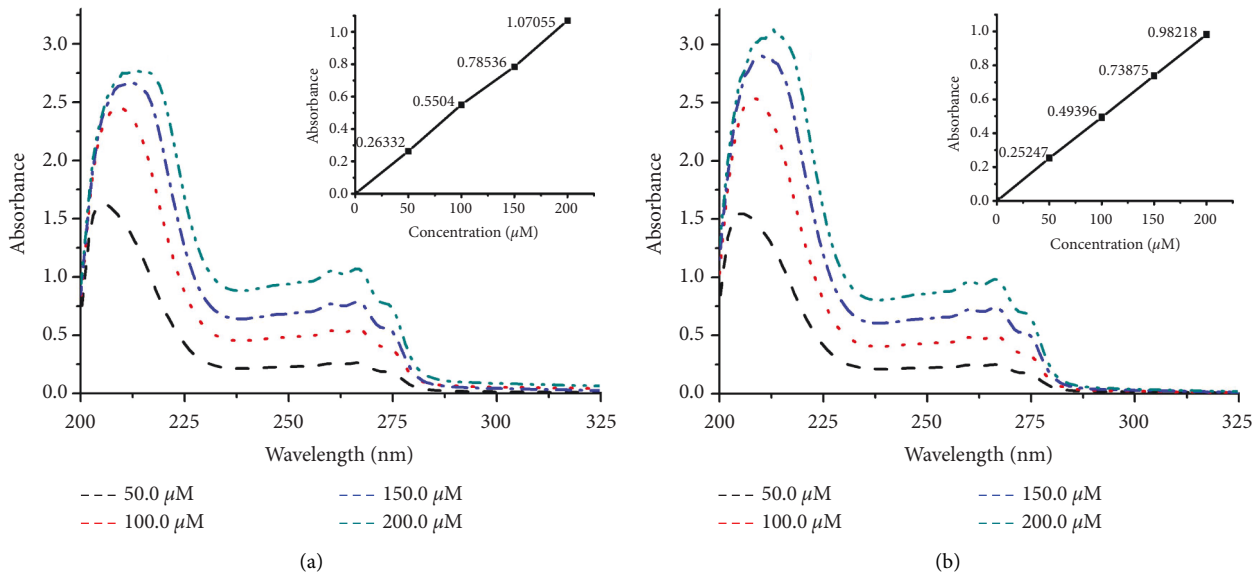

Figure 2: UV-Vis spectra of DBPP in phosphate buffer and 1-octanol at different concentrations: (a) before shaking and (b) after shaking. Insets show the maximum absorbance at 267 nm of DBPP.

Table 3: Cellular uptake of DBPP in U2OS after 24, 48, and 72 h of incubation[a].

Concentration (μM)	Pt content (μg/10^6 cells)		
	24 h	48 h	72 h
50.0	0.6 ± 0.5	0.8 ± 0.9	1.3 ± 0.9
100.0	1.4 ± 0.5	3.7 ± 0.5	5.0 ± 0.3

[a]Treating U2OS cells with cisplatin (10.0 μM) for 24 h resulted in 2.6 ± 0.2 μg/10^6 cells concentration of cellular platinum.

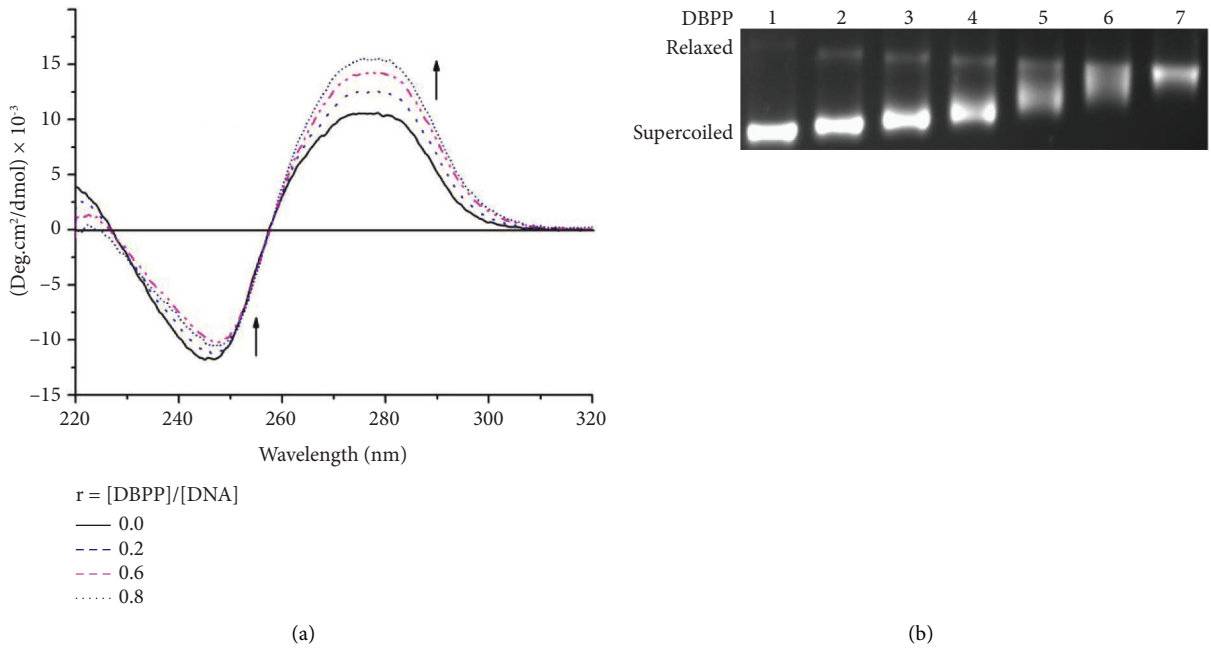

Figure 3: (a) CD spectra of CT-DNA (0.1 mM) in the presence of DBPP at different [BPP]/[DNA] molar ratios after incubation at 37°C for 24 h in buffer (5.0 mM Tris-HCl, 50 mM NaCl, pH 7.4), and (b) agarose gel electrophoresis patterns of pUC19 plasmid DNA incubated with DBPP at 37°C for 24 h Lane 1, DNA control, lanes 2–7, $r_i = 0.30$, 0.60, 0.90, 1.20, 1.50, and 1.60, respectively.

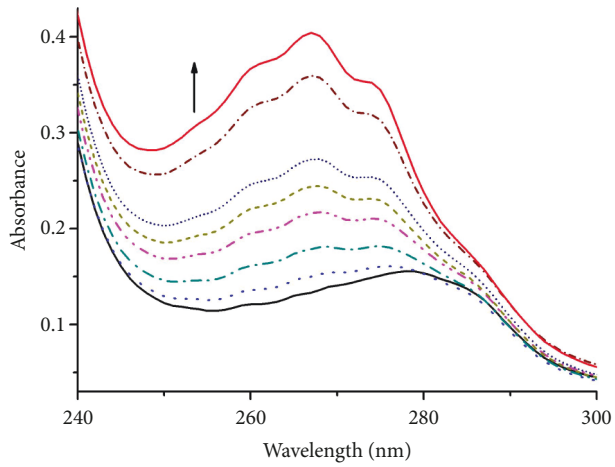

Figure 4: Electronic absorption spectra of HSA (3.0 μM) in the presence of different concentrations of DBPP (0.0, 3.0, 6.0, 12.0, 18.0, 24.0, 30.0, and 48.0 μM). The arrow shows the direction of change in absorbance upon increasing the concentrations of DBPP.

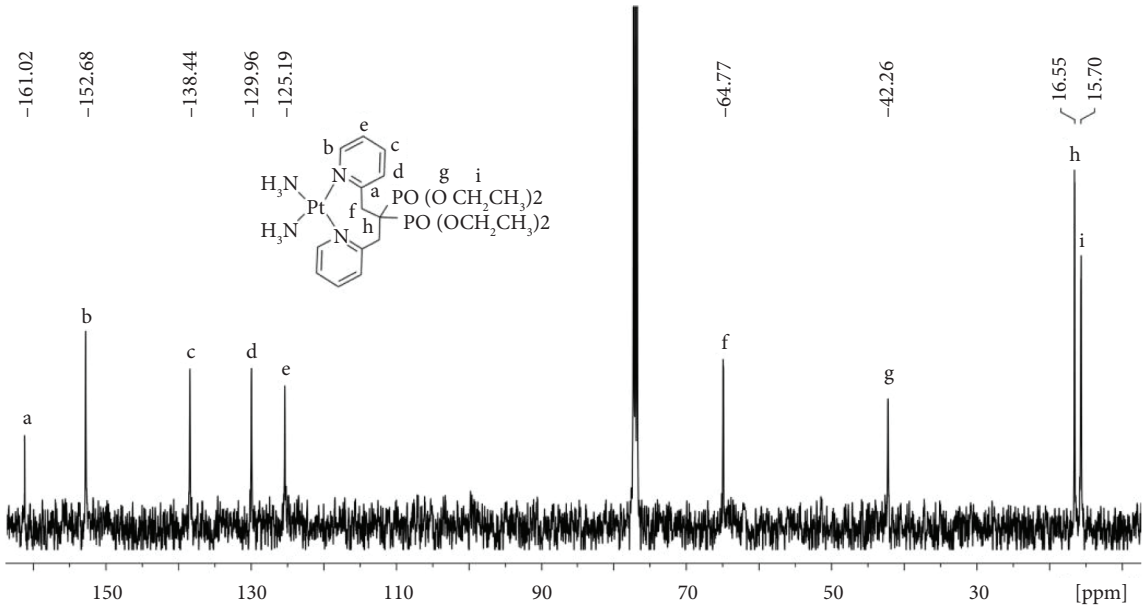

Figure 5: ^{13}C-NMR (125 MHz, $CDCl_3$) spectrum of DBPP.

and weaken the therapeutic efficacy. The interactions between GSH and Pt (II) complexes are therefore considered to play a critical role in mechanisms that are relevant to the inactivation of platinum complexes, their resistance, and side effects [43–45].

Figure 5 demonstrated that DBPP has good solubility in chloroform. Since solubility affects the bioavailability and individual variability of drugs [46], we carried out the solubility test to explore the details of the solubility of DBPP. The solubility values of DBPP in distilled water and chloroform were 0.13 and 0.084 M, respectively. Therefore, the reaction of DBPP with GSH in D_2O was studied at millimolar concentrations at 37°C by ^{31}P NMR and ^{1}H NMR.

As shown in Figure 6(a), the peaks of DBPP are located at 24.88 and 20.09 ppm. After even 168 hours incubation, no obvious changes were observed, indicating that DBPP is quite inert to GSH. Similar results were observed in Figure 6(b). Overall, these results demonstrate that DBPP can hardly chelate with GSH. This is a promising result since GSH-Pt conjugates cannot form, suggesting that DBPP could avoid the GSH-induced side effects. It is worth mentioning that due to the high inertness of GSH, the

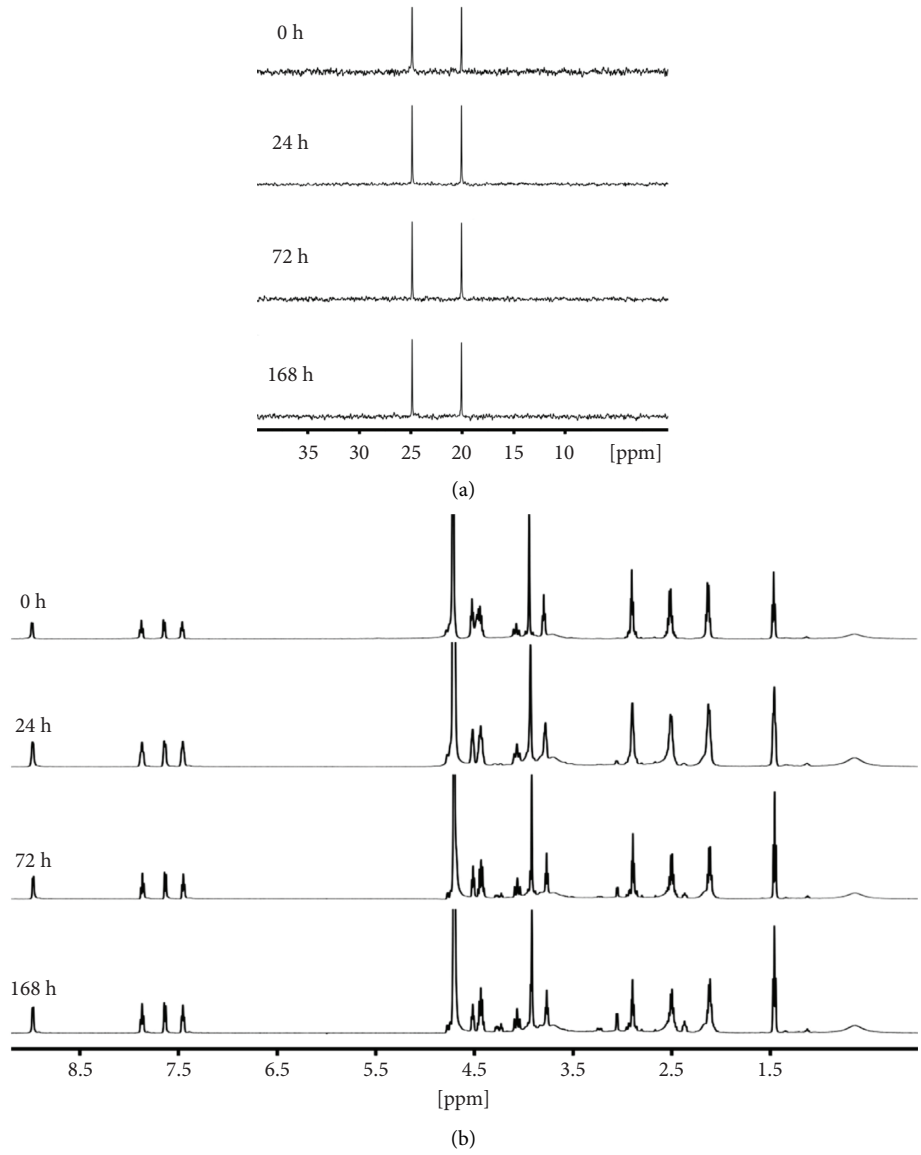

Figure 6: (a) ^{31}P NMR, and (b) ^{1}H NMR spectra at different intervals for DBPP (1.12×10^{-2} M in the presence of GSH 2.64×10^{-2} M at 37°C).

cytotoxicity deficiency of DBPP may be compensated by raising the therapeutic dose.

4. Conclusions

In conclusion, a bisphosphonate platinum complex DBPP was synthesized and characterized. DBPP showed moderate inhibition toward OS cells. The cytostatic action of DBPP is related to the conformational conversion from B-DNA to A-DNA and the unwinding of pUC19 DNA. DBPP could also destroy the tertiary structure of HSA. The objective of this study is to slow down the GSH substitution of platinum complexes. By means of using bulky nitrogen-bisphosphonate and changing the structural motif of complexes, this goal has been basically achieved.

Regardless of the cytotoxicity, these results will open up new avenues to overcome GSH-induced resistance. Our future plans include further activity optimization of BPs-Pt compounds with similar structures, so that BPs-Pt may be used for therapeutic applications in platinum drug resistance.

Data Availability

All data related to this work are presented in the results section along with references.

Conflicts of Interest

The authors declare that they have no conflicts of interest.

Acknowledgments

This work has been supported by the Innovation and Entrepreneurship Program of College Students in Jiangsu (for Zhichao Zhou) and Guizhou Provincial Department of Education Youth Science and Technology Talent Growth Project (no. KY-2018-330).

References

[1] E. Rothzerg, A. L. Pfaff, and S. Koks, "Innovative approaches for treatment of osteosarcoma," *Experimental Biology and Medicine*, vol. 247, no. 4, pp. 310–316, 2022.

[2] P. Maleki Dana, F. Sadoughi, Z. Asemi, and B. Yousefi, "Anti-cancer properties of quercetin in osteosarcoma," *Cancer Cell International*, vol. 21, no. 1, p. 349, 2021.

[3] S. Smeland, S. S. Bielack, J. Whelan et al., "Survival and prognosis with osteosarcoma: outcomes in more than 2000 patients in the EURAMOS-1 (European and American osteosarcoma study) cohort," *European Journal of Cancer*, vol. 109, pp. 36–50, 2019.

[4] M. S. Isakoff, S. S. Bielack, P. Meltzer, and R. Gorlick, "Osteosarcoma: current treatment and a collaborative pathway to success," *Journal of Clinical Oncology*, vol. 33, no. 27, pp. 3029–3035, 2015.

[5] H. D. Dorfman and B. Czerniak, "Bone cancers," *Cancer*, vol. 75, no. S1, pp. 203–210, 1995.

[6] K. Song, J. Song, F. Chen, K. Lin, X. Ma, and J. Jiang, "Prognostic nomograms for predicting overall and cancer-specific survival of high-grade osteosarcoma patients," *Journal of Bone Oncology*, vol. 13, pp. 106–113, 2018.

[7] Y. Zhou, D. Yang, Q. C. Yang et al., "Single-cell RNA landscape of intratumoral heterogeneity and immunosuppressive microenvironment in advanced osteosarcoma," *Nature Communications*, vol. 11, no. 1, 2020.

[8] Y. H. Lin, B. E. Jewell, J. L. Gingold et al., "Osteosarcoma: molecular pathogenesis and ipsc modeling," *Trends in Molecular Medicine*, vol. 23, no. 8, pp. 737–755, 2017.

[9] R. D. Roberts, M. M. Lizardo, D. R. Reed et al., "Provocative questions in osteosarcoma basic and translational biology: a report from the children's oncology group," *Cancer*, vol. 125, no. 20, pp. 3514–3525, 2019.

[10] I. Fernandes, C. Melo-Alvim, R. Lopes-Brás, M. Esperança-Martins, and L. Costa, "Osteosarcoma pathogenesis leads the way to new target treatments," *International Journal of Molecular Sciences*, vol. 22, no. 2, p. 813, 2021.

[11] Y. J. Liu, A. Leng, L. Li et al., "AMTB, a TRPM8 antagonist, suppresses growth and metastasis of osteosarcoma through repressing the TGFβ signaling pathway," *Cell Death & Disease*, vol. 13, no. 3, p. 288, 2022.

[12] N. Martinez-Velez, V. Laspidea, M. Zalacain et al., "Local treatment of a pediatric osteosarcoma model with a 4-1BBL armed oncolytic adenovirus results in an antitumor effect and leads to immune memory," *Molecular Cancer Therapeutics*, vol. 21, no. 3, pp. 471–480, 2022.

[13] J. Du, X. Wang, Y. C. Li et al., "DHA exhibits synergistic therapeutic efficacy with cisplatin to induce ferroptosis in pancreatic ductal adenocarcinoma via modulation of iron metabolism," *Cell Death & Disease*, vol. 12, no. 7, p. 705, 2021.

[14] Y. Jung and S. J. Lippard, "Direct cellular responses to platinum-induced DNA damage," *Chemical Reviews*, vol. 107, no. 5, pp. 1387–1407, 2007.

[15] D. Wang and S. J. Lippard, "Cellular processing of platinum anticancer drugs," *Nature Reviews Drug Discovery*, vol. 4, pp. 307–320, 2005.

[16] Q. Peña, A. Wang, O. Zaremba et al., "Metallodrugs in cancer nanomedicine," *Chemical Society Reviews*, vol. 51, no. 7, pp. 2544–2582, 2022.

[17] C. Y. Zhang, C. Xu, X. Y. Gao, and Q. Q. Yao, "Platinum-based drugs for cancer therapy and anti-tumor strategies," *Theranostics*, vol. 12, no. 5, pp. 2115–2132, 2022.

[18] F. I. Raynaud, F. E. Boxall, P. M. Goddard et al., "cis-Amminedichloro (2-methylpyridine) platinum (II) (AMD473), a novel sterically hindered platinum complex: in vivo activity toxicology, and pharmacokinetics in mice," *Clinical Cancer Research*, vol. 3, pp. 2063–2074, 1997.

[19] S. Kemp, N. J. Wheate, M. J. Pisani, and J. R. Aldrich-Wright, "Degradation of bidentate-coordinated platinum (II)-based DNA intercalators by reduced L-glutathione," *Journal of Medicinal Chemistry*, vol. 51, no. 9, pp. 2787–2794, 2008.

[20] L. A. Graham, G. M. Wilson, T. K. West, C. S. Day, G. L. Kucera, and U. Bierbach, "Unusual reactivity of a potent platinumacridine hybrid antitumor agent," *ACS Medicinal Chemistry Letters*, vol. 2, no. 9, pp. 687–691, 2011.

[21] M. Wang, Y. F. Wu, and C. M. Girgis, "Bisphosphonate drug holidays: evidence from clinical trials and real-world studies," *JBMR Plus (WOA)*, vol. 6, Article ID e10629, 2022.

[22] J. Park, V. R. Pandya, S. J. Ezekiel, and A. M. Berghuis, "Phosphonate and bisphosphonate inhibitors of farnesyl pyrophosphate synthases: a structure-guided perspective," *Frontiers of Chemistry*, vol. 8, Article ID 612728, 2020.

[23] R. A. Nadar, K. Farbod, K. C. V. der Schilden et al., "Targeting of radioactive platinumbisphosphonate anticancer drugs to bone of high metabolic activity," *Scientific Reports*, vol. 10, no. 1, 2020.

[24] K. Farbod, K. Sariibrahimoglu, A. Curci et al., "Controlled release of chemotherapeutic platinum-bisphosphonate complexes from injectable calcium phosphate cements," *Tissue Engineering Part A*, vol. 22, no. 9-10, pp. 788–800, 2016.

[25] Z. Q. Zhang, X. Y. Wang, C. Luo et al., "Dinuclear platinum (II) complexes with bone-targeting groups as potential anti-osteosarcoma agents," *Chemistry–An Asian Journal*, vol. 12, no. 13, pp. 1659–1667, 2017.

[26] Z. Q. Zhang, Z. Z. Zhu, C. Luo et al., "A potential bone-targeting hypotoxic platinum (II) complex with an unusual cytostatic mechanism toward osteosarcoma cells," *Inorganic Chemistry*, vol. 57, no. 6, pp. 3315–3322, 2018.

[27] L. Qiu, H. Yang, G. C. Lv et al., "Insights into the mevalonate pathway in the anticancer effect of a platinum complex on human gastric cancer cells," *European Journal of Pharmacology*, vol. 810, pp. 120–127, 2017.

[28] M. C. Alley, D. A. Scudiero, A. Monks et al., "Feasibility of drug screening with panels of human tumor cell lines using a microculture tetrazolium assay," *Cancer Research*, vol. 48, no. 3, pp. 589–601, 1988.

[29] M. R. Reithofer, A. K. Bytzek, S. M. Valiahdi et al., "Tuning of lipophilicity and cytotoxic potency by structural variation of anticancer platinum (IV) complexes," *Journal of Inorganic Biochemistry*, vol. 105, pp. 3131–3139, 2007.

[30] H. Kong, S. Liu, Y. Shi et al., "Organic-inorganic one-dimensional hybrid aggregates constructed from aromatic-bisphosphonate-functionalized polyoxomolybdates," *Dalton Transactions*, vol. 51, no. 16, pp. 6235–6241, 2022.

[31] H. Frisch, G. Trucks, H. B. Schlegel et al., *Gaussian 09*, Gaussian, Inc, Wallingford, CT, USA, 2009.

[32] V. Fasano, N. Winter, A. Noble, and V. K. Aggarwal, "Divergent, stereospecific mono- and difluoromethylation of boronic esters," *Angewandte Chemie*, vol. 132, no. 22, pp. 8580–8584, 2020.

[33] P. J. Hay and W. R. Wadt, "Ab initio effective core potentials for molecular calculations. Potentials for the transition metal atoms Sc to Hg," *The Journal of Chemical Physics*, vol. 82, no. 1, pp. 270–283, 1985.

[34] M. Maji, S. Karmakar, Ruturaj, A. Gupta, and A. Mukherjee, "Oxamusplatin: a cytotoxic Pt (ii) complex of a nitrogen mustard with resistance to thiol based sequestration displays enhanced selectivity towards cancer," *Dalton Transactions*, vol. 49, no. 8, pp. 2547–2558, 2020.

[35] K. B. Farrell, A. Karpeisky, D. H. Thamm, and S. Zinnen, "Bisphosphonate conjugation for bone specific drug targeting," *BoneKEy Reports*, vol. 9, pp. 47–60, 2018.

[36] K. E. Magomedov, R. Z. Zeynalov, S. I. Suleymanov, S. D. Tataeva, and V. S. Magomedova, "Calculation of lipophilicity of organophosphate pesticides using density functional theory," *Membranes*, vol. 12, no. 6, p. 632, 2022.

[37] M. Kadela-Tomanek, M. Jastrzębska, K. Marciniec, E. Chrobak, E. Bębenek, and S. Boryczka, "Lipophilicity, pharmacokinetic properties, and molecular docking study on SARS-CoV 2 target for betulin triazole derivatives with attached 1, 4-quinone," *Pharmaceutics*, vol. 13, no. 6, p. 781, 2021.

[38] S. P. Oldfield, M. D. Hall, and J. A. Platts, "Calculation of lipophilicity of a large, diverse dataset of anticancer platinum complexes and the relation to cellular uptake," *Journal of Medicinal Chemistry*, vol. 50, no. 21, pp. 5227–5237, 2007.

[39] Y. Zou, B. Van Houten, and N. Farrell, "Ligand effects in platinum binding to DNA. a comparison of DNA binding properties for cis- and trans-[$PtCl_2$(amine)2] (amine = NH_3, pyridine)," *Biochemistry*, vol. 32, no. 37, pp. 9632–9638, 1993.

[40] M. V. Keck and S. J. Lippard, "Unwinding of supercoiled DNA by platinum-ethidium and related complexes," *Journal of the American Chemical Society*, vol. 114, no. 9, pp. 3386–3390, 1992.

[41] S. Paramasivam, K. Kundal, and N. Sarkar, "Human serum albumin aggregation and its modulation using nanoparticles: a review," *Protein and Peptide Letters*, vol. 29, no. 1, pp. 11–21, 2022.

[42] M. D. Aseman, S. Aryamanesh, Z. Shojaeifard, B. Hemmateenejad, and S. M. Nabavizadeh, "Cycloplatinated (II) derivatives of mercaptopurine capable of binding interactions with HSA/DNA," *Inorganic Chemistry*, vol. 58, no. 23, pp. 16154–16170, 2019.

[43] D. Criscuolo, R. Avolio, M. Parri et al., "Decreased levels of GSH are associated with platinum resistance in high-grade serous ovarian cancer," *Antioxidants*, vol. 11, no. 8, p. 1544, 2022.

[44] R. J. Browning, P. J. T. Reardon, M. Parhizkar et al., "Drug delivery strategies for platinum-based chemotherapy," *ACS Nano*, vol. 11, no. 9, pp. 8560–8578, 2017.

[45] S. Liang, L. Q. Han, W. W. Mu et al., "Carboplatin-loaded SMNDs to reduce GSH-mediated platinum resistance for prostate cancer therapy," *Journal of Materials Chemistry B*, vol. 6, no. 43, pp. 7004–7014, 2018.

[46] F. S. Shams Abyaneh, M. Eslami Moghadam, A. Divsalar, D. Ajloo, and M. Hosaini Sadr, "Improving of anticancer activity and solubility of cisplatin by methylglycine and methyl amine ligands against human breast adenocarcinoma cell line," *Applied Biochemistry and Biotechnology*, vol. 186, no. 2, pp. 271–291, 2018.